Supplementary information to On-chip multifunctional metasurfaces with full-parametric multiplexed Jones matrix

Jitao Ji, Jian Li, Zhizhang Wang*, Xueyun Li, Jiacheng Sun, Junyi Wang, Bin Fang, Chen Chen, Xin Ye, Shining Zhu & Tao Li*

National Laboratory of Solid State Microstructures, Key Laboratory of Intelligent Optical Sensing and Manipulations, College of Engineering and Applied Sciences, and Jiangsu Key Laboratory of Artificial Functional Materials, Nanjing University, Nanjing, 210093, China.

**Corresponding authors. Email: zhizhangwang@nju.edu.cn; taoli@nju.edu.cn*

Supplementary Note 1. Comparison of on-chip metasurfaces for guided wave radiation.

Table S1 lists the recent works on on-chip metasurface for guided wave radiation and the corresponding design variables, controllable parameters of equivalent Jones matrix, modulation channels and mechanisms. The equivalent Jones matrix of on-chip metasurface is defined as follows.

$$J=\begin{bmatrix} J_{xx} & J_{yx} \\ J_{xy} & J_{yy} \end{bmatrix}=\begin{bmatrix} A_{xx}\cdot e^{i\varphi_{xx}} & A_{yx}\cdot e^{i\varphi_{yx}} \\ A_{xy}\cdot e^{i\varphi_{xy}} & A_{yy}\cdot e^{i\varphi_{yy}} \end{bmatrix} \tag{S1}$$

Here, A and φ represent the amplitude and phase of each element while the subscripts denote the polarization states of input guided wave and output radiation. Generally speaking, the number of design variables determines the upper limit of independent controllable parameters of equivalent Jones matrix. Regardless of the number of modulation channels which could be additionally increased by complex superposition of multiple phase profiles or optimization algorithms, the controllable parameters of Jones matrix are constraint to be no more than 4 in

essence. To expand the capacity for multiplexing, this work has proposed a supercell design strategy based on detour phase, geometric phase and propagation phase to achieve 12 and 20 design variables, which thus contributes to all eight controllable parameters and direction-multiplexed of Jones matrix. This represents a significant advance in the state-of-the-art metasurfaces for guided wave radiation.

Table S1. Comparison of state-of-the-art on-chip metasurfaces for guided wave radiation.

Reference	Variable	Controllable parameters	Channel	mechanism
Sci. Adv. 6, eabb4142 (2020)	L	φ_{xx}	1	Resonant
Adv. Theory Simul. 4, 2000239 (2021)	δ_x, δ_y	φ_{xx}, φ_{yy}, φ_{-xx}, φ_{-yy}†	4	Detour
Nanophotonics 11, 1923-1930 (2022)	θ	φ_{xL}	1	Geometric
Laser Photonics Rev. 16, 2100638 (2022)	δ_x, δ_y, θ	φ_{xx}, φ_{yy}, φ_{RL}#	3	Detour, Geometric
Optica 9, 670-676 (2022)	δ_x, δ_y	A	4	Detour, Diatom
Nanophotonics 11, 4687-4695 (2022)	L	φ_{xx}	1	Propagation
Nat. Nanotechnol. 18, 580–588 (2023)	δ_1, δ_2, α_1, α_2	A	4	QBIC
Opt. Lett. 48, 3119-3122 (2023)	δ_x, δ_y, θ	φ_{xL}, φ_{xR}, φ_{yy}	3	Detour, Geometric
Photonics Res. 11, 2194-2201 (2023)	θ	φ_{xL}, φ_{xR}	2‡	Geometric
Adv. Funct. Mater. 34, 2312705 (2023)	δ_x, δ_y	φ_{xx}, φ_{yy}, φ_{-xx}, φ_{-yy}†	4‡	Detour
This work	$\boldsymbol{\theta_i}$, $\boldsymbol{\delta_{xi}}$, $\boldsymbol{\delta_{yi}}$ (i=1,2,3,4)	$\boldsymbol{A_{xx}}$, $\boldsymbol{A_{xy}}$, $\boldsymbol{A_{yx}}$, $\boldsymbol{A_{yy}}$, $\boldsymbol{\varphi_{xx}}$, $\boldsymbol{\varphi_{xy}}$, $\boldsymbol{\varphi_{yx}}$, $\boldsymbol{\varphi_{yy}}$	**8***	**Detour, Geometric,**
	$\boldsymbol{L_i}$, $\boldsymbol{W_i}$, $\boldsymbol{\theta_i}$, $\boldsymbol{\delta_{xi}}$, $\boldsymbol{\delta_{yi}}$ (i=1,2,3,4)	$\boldsymbol{\varphi_{\pm xx}}$, $\boldsymbol{\varphi_{\pm xy}}$, $\boldsymbol{\varphi_{\pm yx}}$, $\boldsymbol{\varphi_{\pm yy}}$	**8ξ**	**Detour, Geometric, Propagation**

†phase optimization #free-space channel ‡harmonic strategy

*full-parametric modulation ξdirection-multiplexed modulation

Supplementary Note 2. Derivation of equivalent on-chip Jones matrix

2.1 Jones matrix of on-chip metasurface based on detour phase and geometric phase

In this work, the meta-atoms are selected as nanopillars with C2-symmetry. For on-chip metasurface based on detour phase, the equivalent Jones matrix can be written as

$$J=\begin{bmatrix} J_{xx} & J_{yx} \\ J_{xy} & J_{yy} \end{bmatrix}=\begin{bmatrix} e^{i2\pi\cdot(\delta_y/P_y)} & 0 \\ 0 & e^{i2\pi\cdot(\delta_x/P_x)} \end{bmatrix}\cdot\begin{bmatrix} a_{x0}\cdot e^{i\phi_{x0}} & 0 \\ 0 & a_{y0}\cdot e^{i\phi_{y0}} \end{bmatrix}, \quad (S2)$$
$$=\begin{bmatrix} a_{x0}\cdot e^{i(\phi_{x0}+2\pi\cdot\delta_y/P_y)} & 0 \\ 0 & a_{y0}\cdot e^{i(\phi_{y0}+2\pi\cdot\delta_x/P_x)} \end{bmatrix}$$

where δ_x and δ_y are the position displacements along x and y directions. P_x and P_y represent the effective wavelength of TE_0 guided waves in the slab x-cut LN waveguide along x and y directions. Here, a_{x0}, a_{y0} and ϕ_{x0}, ϕ_{y0} indicate the fixed amplitude and phase responses of the selected nanopillar with constant length L and width W. It can be observed that the Jones matrix in Eq. (S2) is a diagonal matrix that possesses two independent elements J_{xx} and J_{yy}.

In terms of on-chip geometric metasurface, the corresponding Jones matrix is merely related to the rotation angle θ of nanopillar and could be expressed as

$$J=R(\theta)\begin{bmatrix} a_{x0}\cdot e^{i\phi_{x0}} & 0 \\ 0 & a_{y0}\cdot e^{i\phi_{y0}} \end{bmatrix}R(-\theta)$$
$$=\begin{bmatrix} \cos^2\theta\cdot a_{x0}\cdot e^{i\phi_{x0}}+\sin^2\theta\cdot a_{y0}\cdot e^{i\phi_{y0}} & \sin\theta\cdot\cos\theta\cdot(a_{x0}\cdot e^{i\phi_{x0}}-a_{y0}\cdot e^{i\phi_{y0}}) \\ \sin\theta\cdot\cos\theta\cdot(a_{x0}\cdot e^{i\phi_{x0}}-a_{y0}\cdot e^{i\phi_{y0}}) & \sin^2\theta\cdot a_{x0}\cdot e^{i\phi_{x0}}+\cos^2\theta\cdot a_{y0}\cdot e^{i\phi_{y0}} \end{bmatrix},$$

$$\text{where}\quad R(\theta)=\begin{bmatrix} \cos\theta & -\sin\theta \\ \sin\theta & \cos\theta \end{bmatrix}. \quad (S3)$$

Since there is only one variable θ in Eq. (S3), the number of controllable elements in Jones matrix based on geometric phase is one (e.g. J_{xx}).

Through combining detour phase and geometric phase, the equivalent Jones matrix of on-chip metasurface could be derived as

$$J = \begin{bmatrix} e^{i2\pi\cdot(\delta_y/P_y)} & 0 \\ 0 & e^{i2\pi\cdot(\delta_x/P_x)} \end{bmatrix} R(\theta) \begin{bmatrix} a_{x0}\cdot e^{i\phi_{x0}} & 0 \\ 0 & a_{y0}\cdot e^{i\phi_{y0}} \end{bmatrix} R(-\theta)$$
$$= \begin{bmatrix} \cos^2\theta\cdot a_{x0}\cdot e^{i(\phi_{x0}+2\pi\cdot\delta_y/P_y)} + \sin^2\theta\cdot a_{y0}\cdot e^{i(\phi_{y0}+2\pi\cdot\delta_y/P_y)} & \sin\theta\cdot\cos\theta\cdot(a_{x0}\cdot e^{i\phi_{x0}} - a_{y0}\cdot e^{i\phi_{y0}})\cdot e^{i2\pi\cdot(\delta_x/P_x)} \\ \sin\theta\cdot\cos\theta\cdot(a_{x0}\cdot e^{i\phi_{x0}} - a_{y0}\cdot e^{i\phi_{y0}})\cdot e^{i2\pi\cdot(\delta_y/P_y)} & \sin^2\theta\cdot a_{x0}\cdot e^{i(\phi_{x0}+2\pi\cdot\delta_x/P_x)} + \cos^2\theta\cdot a_{y0}\cdot e^{i(\phi_{y0}+2\pi\cdot\delta_x/P_x)} \end{bmatrix} \quad \text{, (S4)}$$

Here, a_{x0}=0.15, a_{y0}=0.02 and ϕ_{x0}=-1.38, ϕ_{y0}=-2.28 are the amplitude and phase responses of the selected nanopillar with L=300 nm and W=100 nm. It is noted that the introduction of detour phase makes the Jones matrix asymmetric, that is $J_{xy}\neq J_{yx}$. Besides, on account that a_{x0} is much larger than a_{y0}, the Jones matrix expressed in Eq. (S2) is nearly unitary, namely $J^{-1}\approx J^{H}$. Such unitary condition makes the four elements of Jones matrix correlative by $J_{xx}\cdot J_{xy}^{*} + J_{yx}\cdot J_{yy}^{*} = 0$ (* represents complex conjugation) and leads to 3 independent elements.

With the arrangement of four-element supercell, the Jones matrix could be derived as follows according to the interference effect of meta-atoms (k is the sequence of the nanopillar in a four-element supercell).

$$J = \sum_{k=1}^{4} \begin{bmatrix} \cos^2\theta_k\cdot a_{x0}\cdot e^{i(\phi_{x0}+2\pi\cdot\delta_{yk}/P_y)} + \sin^2\theta_k\cdot a_{y0}\cdot e^{i(\phi_{y0}+2\pi\cdot\delta_{yk}/P_y)} & \sin\theta_k\cdot\cos\theta_k\cdot(a_{x0}\cdot e^{i\phi_{x0}} - a_{y0}\cdot e^{i\phi_{y0}})\cdot e^{i2\pi\cdot(\delta_{xk}/P_x)} \\ \sin\theta_k\cdot\cos\theta_k\cdot(a_{x0}\cdot e^{i\phi_{x0}} - a_{y0}\cdot e^{i\phi_{y0}})\cdot e^{i2\pi\cdot(\delta_{yk}/P_y)} & \sin^2\theta_k\cdot a_{x0}\cdot e^{i(\phi_{x0}+2\pi\cdot\delta_{xk}/P_x)} + \cos^2\theta_k\cdot a_{y0}\cdot e^{i(\phi_{y0}+2\pi\cdot\delta_{xk}/P_x)} \end{bmatrix} \quad \text{(S5)}$$

Since $J\neq J^{T}$ and $J^{-1}\neq J^{H}$, the above Jones matrix is asymmetric and non-unitary, contributing to all the four elements independent and full-parametric modulation.

2.2 Jones matrix of on-chip metasurface based on detour phase, geometric phase and propagation phase

With regard to direction-multiplexed modulation, the Jones matrices $J_{\pm}$ for forward- and backward-propagating guided waves can be described as below when taking propagation phase into consideration.

$$J_{\pm}=\sum_{k=1}^{4}\begin{bmatrix}\cos^2\theta_k\cdot a_{xk}\cdot e^{i(\phi_{xk}\pm 2\pi\cdot\delta_{yk}/P_y)}+\sin^2\theta_k\cdot a_{yk}\cdot e^{i(\phi_{yk}\pm 2\pi\cdot\delta_{yk}/P_y)} & \sin\theta_k\cdot\cos\theta_k\cdot(a_{xk}\cdot e^{i\phi_{xk}}-a_{yk}\cdot e^{i\phi_{yk}})\cdot e^{\pm i2\pi\cdot(\delta_{xk}/P_x)}\\ \sin\theta_k\cdot\cos\theta_k\cdot(a_{xk}\cdot e^{i\phi_{xk}}-a_{yk}\cdot e^{i\phi_{yk}})\cdot e^{\pm i2\pi\cdot(\delta_{yk}/P_y)} & \sin^2\theta_k\cdot a_{xk}\cdot e^{i(\phi_{xk}\pm 2\pi\cdot\delta_{xk}/P_x)}+\cos^2\theta_k\cdot a_{yk}\cdot e^{i(\phi_{yk}\pm 2\pi\cdot\delta_{xk}/P_x)}\end{bmatrix} \tag{S6}$$

Here, a_{xk}, a_{yk} and ϕ_{xk}, ϕ_{yk} are the amplitude and phase responses of induced propagation phase of the k-th nanopillar. Figure S1a and S1b illustrate the extracted efficiency T_x and T_y of guided waves as a function of length and width of single nanopillar for guided waves propagating along y and x directions. Thus, the amplitude response a_x and a_y of nanopillar can be obtained according to $a_x=\sqrt{T_x}$ and $a_y=\sqrt{T_y}$. It is observed that the conjugated relation is broken since $J_+\neq J_-^*$ and therefore J_+ is totally independent on J_-.

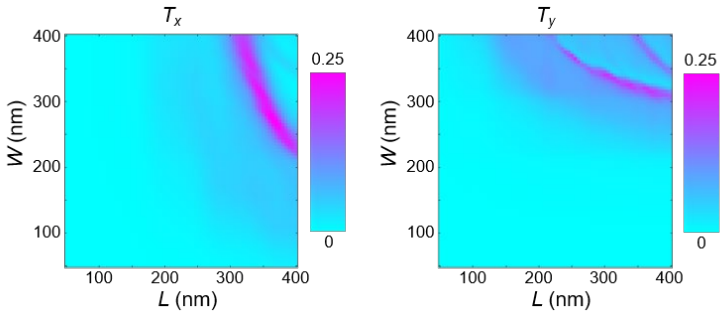

Fig. S1 The extracted efficiency (a) T_x and (b) T_y as a function of the length and width of nanopillar under input guided waves along y and x directions.

Supplementary Note 3. Design flow of genetic algorithm optimization

To determine the variables of nanopillars in each supercell, genetic algorithm is employed to solve the corresponding linear equations for both full-parametric and direction-multiplexed modulation of Jones matrix.

First, to achieve arbitrary amplitude (A_1, A_2, A_3, A_4) and phase (φ_1, φ_2, φ_3, φ_4) distributions for full-parametric modulation, the following equations are required to be satisfied.

$$
\begin{aligned}
&|J_{xx}| = A_1, \arg(J_{xx}) = \varphi_1 \\
&|J_{xy}| = A_2, \arg(J_{xy}) = \varphi_2 \\
&|J_{yx}| = A_3, \arg(J_{yx}) = \varphi_3 \\
&|J_{yy}| = A_4, \arg(J_{yy}) = \varphi_4
\end{aligned}
\tag{S7}
$$

In order to avoid overlapping of nanopillars, the constraint conditions on spatial arrangement of nanopillars should be added during the process of solving Eqs. (S7), which can be described as the following inequalities.

$$
\begin{aligned}
&0 < \delta_x < 1.5P_x, 0 < \delta_y < 1.5P_y \\
&(\delta_{xm} - \delta_{xn})^2 + (\delta_{ym} - \delta_{yn})^2 > d^2 \\
&where\ m, n = 1, 2, 3, 4\ and\ m \neq n
\end{aligned}
\tag{S8}
$$

Figure S2 lists the design flow of genetic algorithm optimization process. First of all, the targeted amplitude and phase distributions with 60×60 pixels are obtained through Gerchberg–Saxton (G-S) algorithm (See Fig. S3 in Supplementary Note 4). For each pixel, the iteration procedure starts with the initialized population of variables as the original generation with the constraint that the displacement δ_x and δ_y of each nanopillar is within 0~1.5P_x and 0~1.5P_y while the separation between each nanopillar is over d=500 nm. Then, the fitness function is evaluated by calculating the sum of mean-square errors (MSE) between the constructed Jones matrix J and the targets $A_i^t \cdot e^{i\varphi_i^t}$. The next generation will subsequently be generated through selection, crossover and mutation. Such evolution process cycles until the terminate condition is satisfied. Eventually, the optimized 12 variables (θ_k, δ_{xk}, δ_{yk}, k=1,2,3,4) are found for full-parametric modulation of Jones matrix. After optimization for all the 60×60 pixels, the four sets of nano-printing and holographic images can be reconstructed as shown in Fig. S5a.

In addition, for direction-multiplexed modulation of Jones matrix to obtain arbitrary eight phase-only channels, the following equations should be solved with the same constraint conditions expressed by inequalities S8.

$$\begin{aligned}
&\arg(J_{+xx}) = \varphi_1, \arg(J_{+yx}) = \varphi_2 \\
&\arg(J_{+xy}) = \varphi_3, \arg(J_{+yy}) = \varphi_4 \\
&\arg(J_{-xx}) = \varphi_5, \arg(J_{-yx}) = \varphi_6 \\
&\arg(J_{-xy}) = \varphi_7, \arg(J_{-yy}) = \varphi_8
\end{aligned} \tag{S9}$$

Here, φ_1 to φ_8 represent the phase distributions of targeted holographic images, which are plotted in Fig. S4. The optimization process is described in Fig. S2 and the 20 variables of nanopillars (θ_k, δ_{xk}, δ_{yk}, L_k, W_k, k=1,2,3,4) in each supercell could be achieved once the optimization loop is terminated. The reconstructed far-field holographic images were plotted in Fig. S6a, in accordance with the targets.

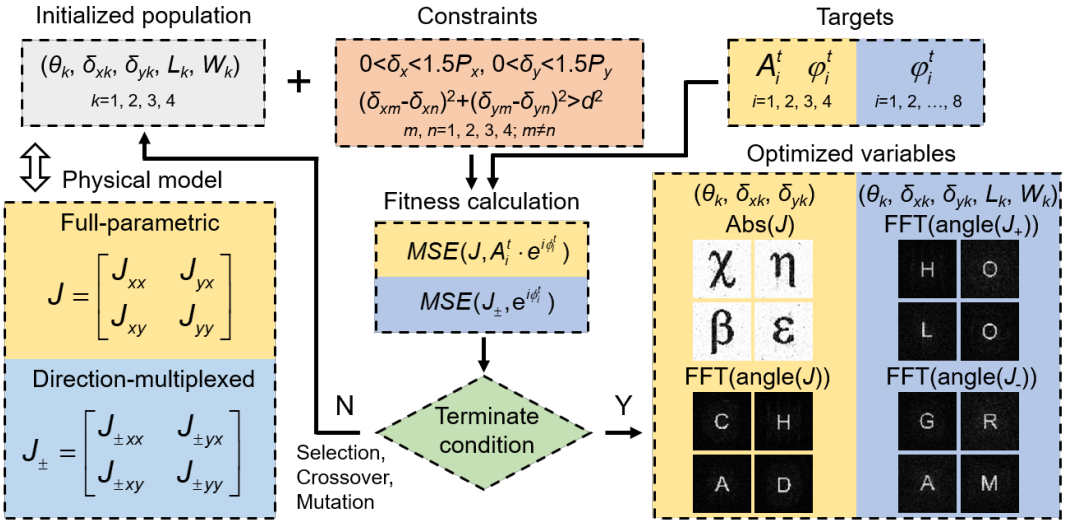

Fig. S2 The design flow of genetic algorithm to determine the variables of four-element supercell for full-parametric and direction-multiplexed modulation of Jones matrix.

Supplementary Note 4. The targeted, theoretical and simulated amplitude and phase distributions

Figure S3 presents four sets of targeted amplitude and phase distributions with 60×60 pixels generated through Gerchberg–Saxton (G-S) algorithm for full-parametric modulation of Jones matrix. The third row exhibits the reconstructed holographic images according to the

above amplitude and phase distributions. Similarly, the targeted phase distributions with 60×60 pixels for eight phase-only channels to modulate the eight parameters of direction-multiplexed modulation of Jones matrix are demonstrated in Fig. S4.

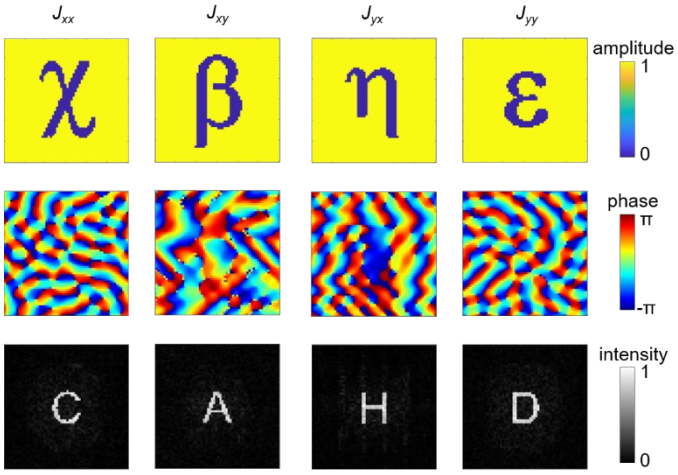

Fig. S3 The four sets of targeted amplitude, phase distributions and holographic images for full-parametric modulation of Jones matrix.

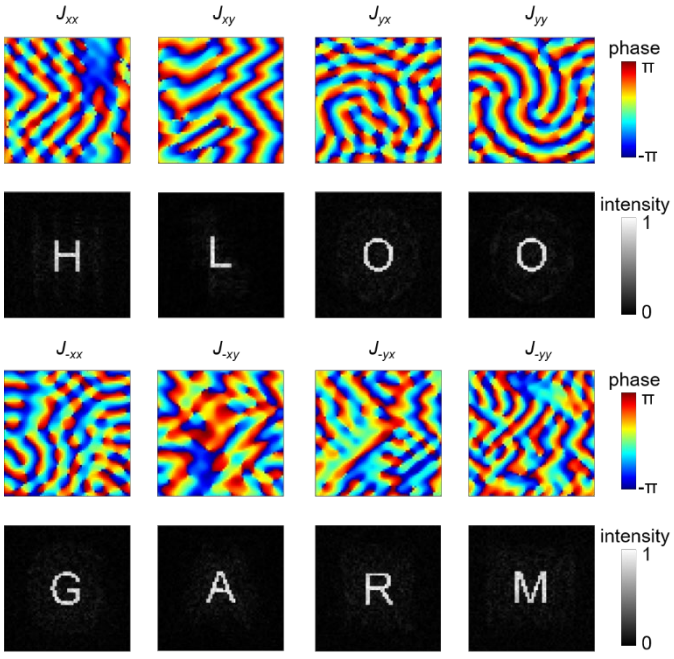

Fig. S4 The eight targeted phase distributions and corresponding holographic images for direction-multiplexed modulation of Jones matrix.

To demonstrate the accuracy of Eqs. (3) and (4) in the main text, we have performed full-wave simulations to compare with the theoretical results after genetic algorithm optimization. Figure S5a and S5b present the optimized results through genetic algorithm and the simulated nano-printing images, phase profiles and holographic images, respectively. It is clear that the simulation results are in agreement with the optimized ones. Similarly, the validity of direction-multiplexed modulation design (i.e., Eq. (4)) has been confirmed by comparing the theoretical and simulated phase profiles and holographic images listed in Fig. S6.

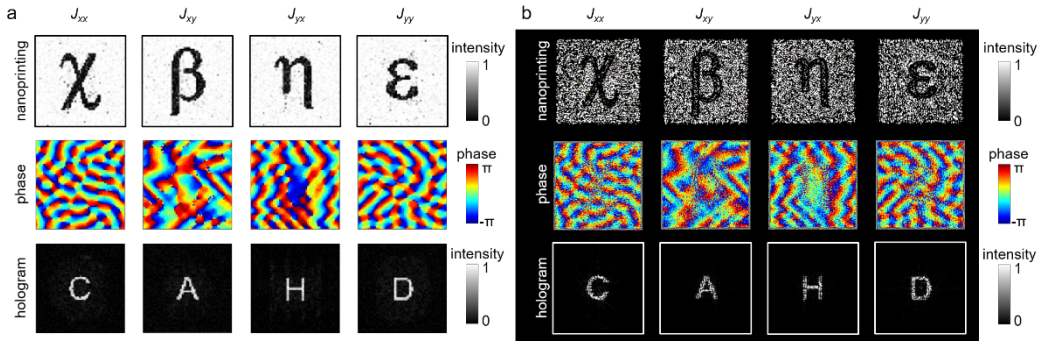

Fig. S5 (a) The optimized results through genetic algorithm and (b) the full-wave simulation results for full-parametric modulation of Jones matrix.

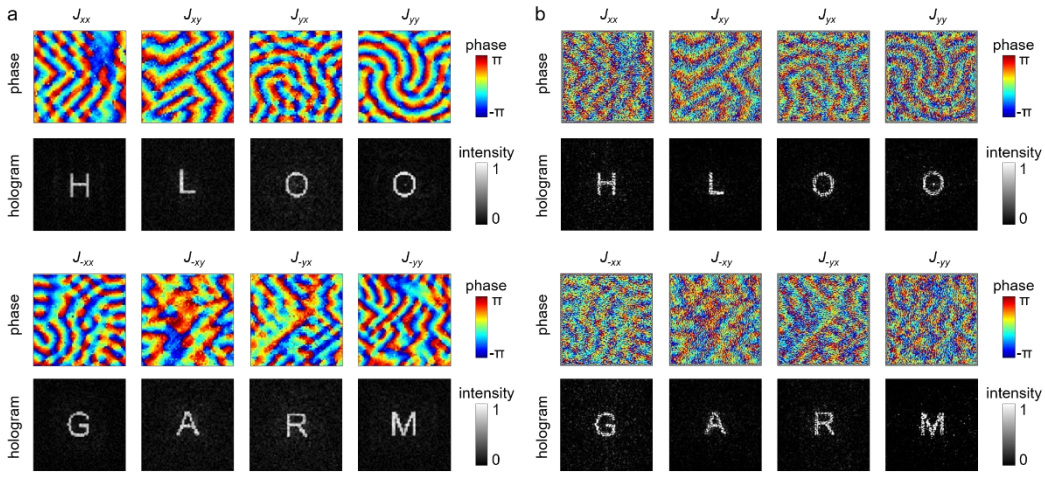

Fig. S6 Comparison between (a) the optimized and (b) the full-wave simulation results for direction-multiplexed modulation of Jones matrix.

Supplementary Note 5. Experimental setup

The experimental setup to characterize the on-chip metasurface is schematically illustrated in Fig. S7. An incident 1550 nm laser with polarization states controlled by a polarizer was focused onto the grating couplers through objective 1 to excite TE_0 modes in slab LN waveguide. By switching the illuminated four grating couplers surrounding the on-chip metasurface, the guided waves propagating along x, y, -x and -y directions could be obtained. Subsequently, the guided wave radiations extracted by on-chip metasurface were collected as nano-printing images in the objective plane by objective 2 (50×, NA=0.42) and a near-infrared CCD. To acquire holographic images, a Fourier lens indicated by the dashed box in Fig. S7 was placed in front of the CCD to perform Fourier transformation of objective plane and the CCD was used to capture the intensity distributions in the Fourier plane. All the collected images were characterized by polarization analyzer to obtain the output polarization properties.

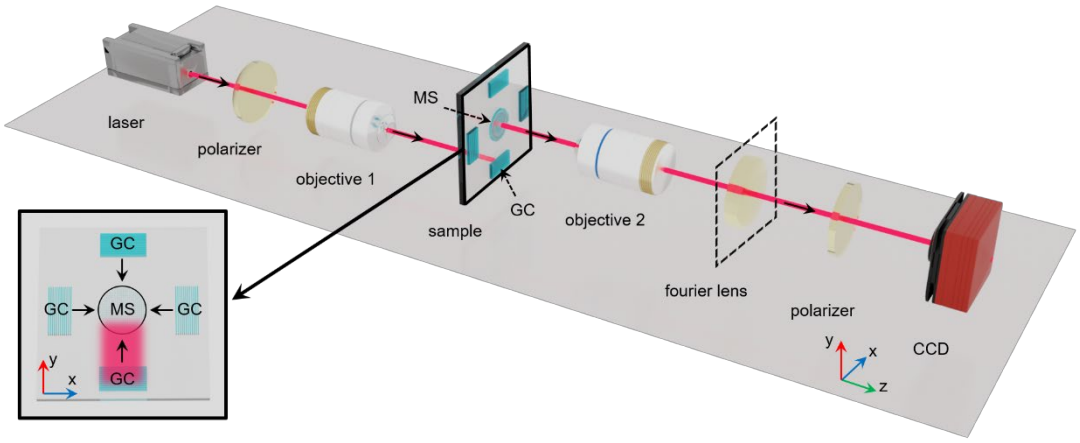

Fig. S7 Illustration of measurement setup in experiments. The inset shows the diagram of the sample and the guided wave propagating along y direction excited through one GC. GC: grating coupler. MS: metasurface. CCD: charge coupled device.

Supplementary Note 6. Full-parametric modulation of Jones matrix for arbitrary set of polarization states

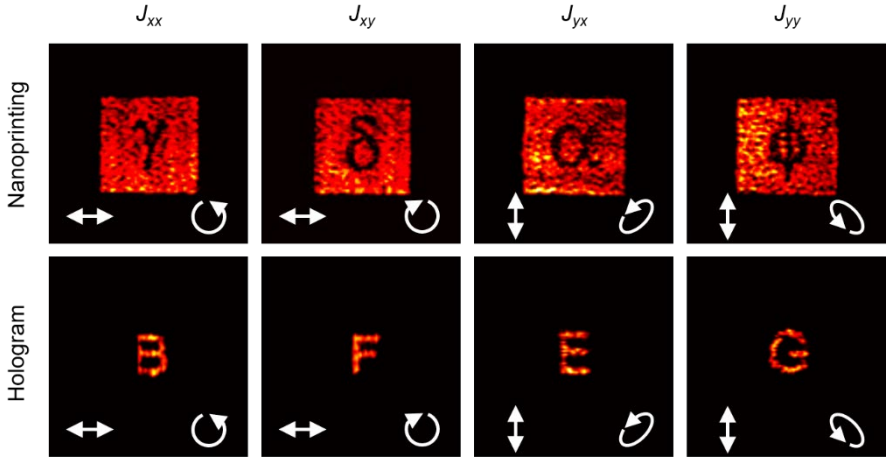

Fig. S8 Independent amplitude and phase control of arbitrary set of output polarization states. The white arrows in the bottom left and right corner indicate the polarization states of input guided waves and output analyzers.

In addition to linearly polarized output channels, the proposed on-chip metasurface based on detour phase and geometric phase is also applicable for arbitrary set of output polarization states. Assuming that the four output channels are $\alpha_1 = \begin{bmatrix} \gamma_1 \\ \gamma_2 \end{bmatrix}$, $\alpha_2 = \begin{bmatrix} \eta_1 \\ \eta_2 \end{bmatrix}$, $\beta_1 = \begin{bmatrix} \mu_1 \\ \mu_2 \end{bmatrix}$ and $\beta_2 = \begin{bmatrix} \nu_1 \\ \nu_2 \end{bmatrix}$ with independent amplitude and phase control of $A_1 \cdot e^{i\varphi_1}$, $A_2 \cdot e^{i\varphi_2}$, $A_3 \cdot e^{i\varphi_3}$ and $A_4 \cdot e^{i\varphi_4}$, the equivalent Jones matrix should satisfy

$$J \cdot \begin{bmatrix} 1 \\ 0 \end{bmatrix} = A_1 \cdot e^{i\varphi_1} \begin{bmatrix} \gamma_1 \\ \gamma_2 \end{bmatrix} + A_2 \cdot e^{i\varphi_2} \begin{bmatrix} \eta_1 \\ \eta_2 \end{bmatrix} \tag{S10}$$

$$\text{and} \quad J \cdot \begin{bmatrix} 0 \\ 1 \end{bmatrix} = A_3 \cdot e^{i\varphi_3} \begin{bmatrix} \mu_1 \\ \mu_2 \end{bmatrix} + A_4 \cdot e^{i\varphi_4} \begin{bmatrix} \nu_1 \\ \nu_2 \end{bmatrix}. \tag{S11}$$

Hence, the Jones matrix writes

$$J=\begin{bmatrix} A_1\cdot e^{i\varphi_1}\gamma_1+A_2\cdot e^{i\varphi_2}\eta_1 & A_3\cdot e^{i\varphi_3}\mu_1+A_4\cdot e^{i\varphi_4}\nu_1 \\ A_1\cdot e^{i\varphi_1}\gamma_2+A_2\cdot e^{i\varphi_2}\eta_2 & A_3\cdot e^{i\varphi_3}\mu_1+A_4\cdot e^{i\varphi_4}\nu_1 \end{bmatrix}. \tag{S12}$$

Without loss of generality, we choose two circular polarization $\alpha_1=\frac{\sqrt{2}}{2}\begin{bmatrix}1\\ i\end{bmatrix}$, $\alpha_2=\frac{\sqrt{2}}{2}\begin{bmatrix}1\\ -i\end{bmatrix}$ and two elliptical polarization $\beta_1=\frac{\sqrt{2}}{2}\begin{bmatrix}1\\ \frac{1+i}{\sqrt{2}}\end{bmatrix}$, $\beta_2=\frac{\sqrt{2}}{2}\begin{bmatrix}-1\\ \frac{1+i}{\sqrt{2}}\end{bmatrix}$ as four output polarization states. Figure S8 displays the measured four sets of nanoprinting and holographic images, which verifies the feasibility of full-parametric modulation for arbitrary set of output polarization channels.

Supplementary Note 7. The conjugated relation of Jones matrices for forward- and backward-propagating guided waves

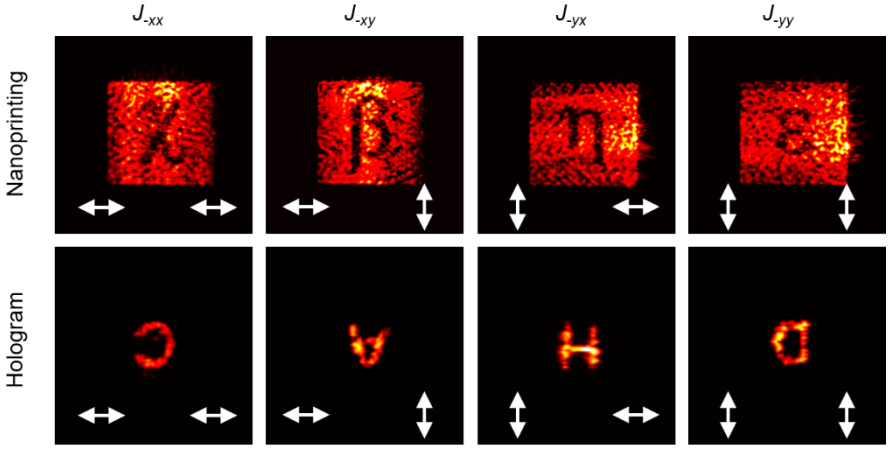

Fig. S9 The captured nano-printing and holographic images corresponding to four elements of Jones matrix J_{-xx}, J_{-xy}, J_{-yy} and J_{-yy} under input guided waves propagating along -y and -x directions. The white arrows in the bottom left and right corner indicate the polarization states of input guided waves and output analyzers.

For the on-chip metasurface based on detour phase and geometric phase, the Jones matrices $J_{\pm}$ under forward- and backward-propagating guided waves can be written as follows according to Eq. (S5).

$$J_{\pm}=\sum_{k=1}^{4}\begin{bmatrix}\cos^2\theta_k\cdot a_{x0}\cdot e^{i(\phi_{x0}\pm 2\pi\cdot\delta_{yk}/P_y)}+\sin^2\theta_k\cdot a_{y0}\cdot e^{i(\phi_{y0}\pm 2\pi\cdot\delta_{yk}/P_y)} & \sin\theta_k\cdot\cos\theta_k\cdot(a_{x0}\cdot e^{i\phi_{x0}}-a_{y0}\cdot e^{i\phi_{y0}})\cdot e^{\pm i2\pi\cdot(\delta_{xk}/P_x)}\\ \sin\theta_k\cdot\cos\theta_k\cdot(a_{x0}\cdot e^{i\phi_{x0}}-a_{y0}\cdot e^{i\phi_{y0}})\cdot e^{\pm i2\pi\cdot(\delta_{yk}/P_y)} & \sin^2\theta_k\cdot a_{x0}\cdot e^{i(\phi_{x0}\pm 2\pi\cdot\delta_{xk}/P_x)}+\cos^2\theta_k\cdot a_{y0}\cdot e^{i(\phi_{y0}\pm 2\pi\cdot\delta_{xk}/P_x)}\end{bmatrix} \tag{S13}$$

Noting that a_{x0}=0.15 is much larger than a_{y0}=0.02, the above two Jones matrices obey the approximate conjugated relation of $J_{+}=J_{-}^{*}$. To validate such conjugated relation, we experimentally investigate the equivalent Jones matrices under backward-propagating guided waves. Figure S9 shows the measured nano-printing and holographic images when the guided waves are excited along -y and -x directions, corresponding to the four elements J_{-xx}, J_{-xy}, J_{-yx} and J_{-yy}. Compared with Fig.3 in the main text, the four nano-printing images present the same intensity distributions but the holographic images are centrosymmetric with those in Fig.3, since the amplitude of each element in Jones matrix remains unchanged while the phase of each element is opposite when the propagation direction of input guided wave is reversed. Therefore, the conjugated relation of Jones matrices for forward- and backward-propagating guided waves has been verified.

Supplementary Note 8. Combination of direction-multiplexed modulation with harmonic strategy and z-plane spatial multiplexing

As proof of concept, we combine the direction-multiplexed modulation design with complex superposition of multiple phase profiles and z-plane spatial multiplexing to demonstrate 32 focal points through a single on-chip metasurface via numerical simulation.

The detailed phase distributions of eight phase channels are designed as

$$\arg(J_{+xx}) = \sum_{j=1}^{4} e^{i\varphi^{z_j}_{x_1,y_1}}, \arg(J_{+yx}) = \sum_{j=1}^{4} e^{i\varphi^{z_j}_{x_3,y_3}}$$

$$\arg(J_{+xy}) = \sum_{j=1}^{4} e^{i\varphi^{z_j}_{x_2,y_2}}, \arg(J_{+yy}) = \sum_{j=1}^{4} e^{i\varphi^{z_j}_{x_4,y_4}}$$

$$\arg(J_{-xx}) = \sum_{j=1}^{4} e^{i\varphi^{z_j}_{x_5,y_5}}, \arg(J_{-yx}) = \sum_{j=1}^{4} e^{i\varphi^{z_j}_{x_7,y_7}}$$

$$\arg(J_{-xy}) = \sum_{j=1}^{4} e^{i\varphi^{z_j}_{x_6,y_6}}, \arg(J_{-yy}) = \sum_{j=1}^{4} e^{i\varphi^{z_j}_{x_8,y_8}}$$

$$where \ \varphi^{z_j}_{x_{1-8},y_{1-8}} = \frac{2\pi}{\lambda} \cdot \left(\sqrt{x_{1-8}^2 + y_{1-8}^2 + z_j^2} - \sqrt{(x - x_{1-8})^2 + (y - y_{1-8})^2 + z_j^2}\right). \quad \text{(S14)}$$

Here, $x_{1\text{-}8}$ and $y_{1\text{-}8}$ denote the horizontal and vertical coordinates of focal points while z_j represents the multiplexed z-plane. As illustrated in Fig. S10, for +x, +y, -x and -y direction illuminations, the simulated 32 focal points are located at different spatial positions at four z-planes (z=50 μm, 75 μm, 100 μm and 125 μm) as designed. The above results demonstrate the compatibility of the proposed design for parameter modulation of Jones matrix with other strategies to achieve more number of channels with improved multiplexing capability.

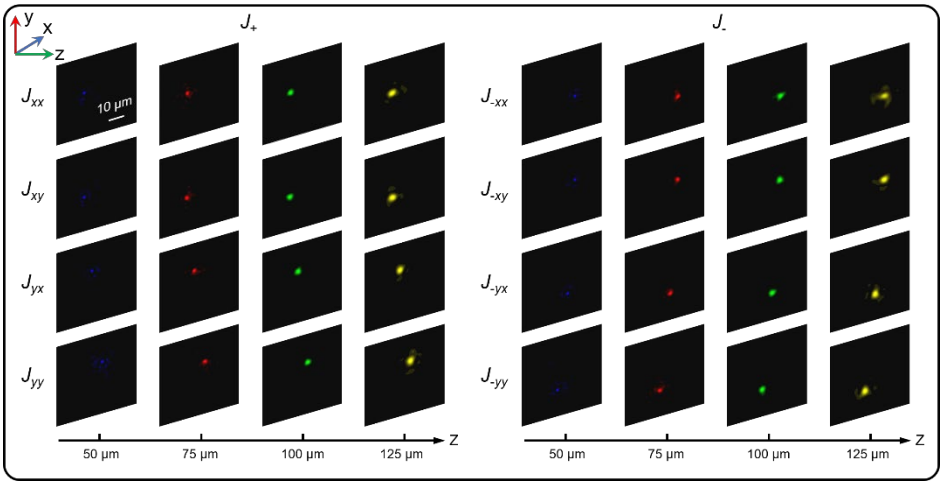

Fig. S10 Direction-multiplexed modulation combined with harmonic strategy and z-plane spatial multiplexing for generating 32-channel multiplexed focal points.